

**Experimental violation of the Leggett-Garg inequality in a three-level trapped-ion system**Tianxiang Zhan <sup>1,2,3,\*</sup>, Chunwang Wu,<sup>1,2,3,\*</sup> Manchao Zhang,<sup>1,2,3</sup> Qingqing Qin <sup>1,2,3</sup>, Xueying Yang,<sup>1,2,3</sup> Han Hu,<sup>1,2,3</sup> Wenbo Su <sup>1,2,3</sup>, Jie Zhang <sup>1,2,3</sup>, Ting Chen <sup>1,2,3</sup>, Yi Xie <sup>1,2,3</sup>, Wei Wu,<sup>1,2,3,4,†</sup> and Pingxing Chen <sup>1,2,3,4</sup><sup>1</sup>*Institute for Quantum Science and Technology, College of Science, National University of Defense Technology, Changsha Hunan 410073, China*<sup>2</sup>*Hunan Key Laboratory of Mechanism and Technology of Quantum Information, Changsha Hunan 410073, China*<sup>3</sup>*Interdisciplinary Center for Quantum Information, National University of Defense Technology, Changsha Hunan 410073, China*<sup>4</sup>*Hefei National Laboratory, Hefei 230088, PR China*

(Received 15 September 2022; accepted 23 December 2022; published 25 January 2023)

Leggett-Garg inequality (LGI) is used to detect whether the macroscopic superposition state exists. Classical systems obey the LGI, but quantum systems may violate it. In the multilevel system, different state update rules determine different upper bounds of LGI. In this work, we experimentally test the LGI in a three-level trapped-ion system under the Lüders and the von Neumann state update rules, respectively. The maximum observed value of the Leggett-Garg correlator under the von Neumann state update rule is  $K_3 = 1.739 \pm 0.014$ , which demonstrates a violation of the Lüders bound by 17 standard deviations and is by far the most significant violation under the specific model. The method used in our experiment could also be used in other multilevel experiments in the trapped-ion system.

DOI: [10.1103/PhysRevA.107.012424](https://doi.org/10.1103/PhysRevA.107.012424)**I. INTRODUCTION**

One of the most counterintuitive features of quantum mechanics is the superposition of quantum states [1]. In 1935, Schrödinger extended the superposition from the micro world to the macro world through the thought experiment of Schrödinger's cat [2]. However, it seems to contradict the fact that objects in our daily life are always in a certain state. According to this contradiction, in 1985, Leggett and Garg proposed the Leggett-Garg inequality (LGI) based on two fundamental assumptions of the macro world [3]: (A1) Macroscopic realism (MR): A macroscopic system is always in one of the macroscopically distinct states; (A2) Noninvasive measurability (NIM) at the macroscopic level: A determination method can be found that does not affect the past and the future of the system [3]. Because these two assumptions are invalid in quantum mechanics, quantum systems may violate the LGI.

Based on the above two assumptions, the standard LGI is

$$-3 \leq K_3 \leq 1, \quad (1)$$

where  $K_3$  is a linear combination of temporal correlations of observables measured sequentially at different moments [4]. The upper bound 1 is usually called the classical bound (CB), which limits the behavior of classical systems. For two-dimensional quantum systems, the maximum value of  $K_3$  is 1.5 [3], which is usually called the Lüders bound (LB) [4] (this bound is also called the temporal Tsirelson bound (TTB) [5–7]). For higher-dimensional quantum systems, it has been strictly proved that the maximum value of  $K_3$  is still 1.5 [8]

under the Lüders state update rule (LSUR) [9]. Later, Budroni and Emery proved that  $K_3$  might exceed 1.5 in systems with three or more dimensions under the von Neumann state update rule (VSUR) [10], and the maximum value of  $K_3$  increases with increasing dimension, which can approach 3, the algebraic bound [4].

In 2010, Palacios-Laloy announced the first experimental violation of LGI [11]. Subsequently, several experimental tests of LGI in two-level quantum systems were reported, including the single-photon system [12], the spin-bearing phosphorus impurities in silicon system [13], the nuclear magnetic resonance system [14], the superconducting system [15], etc. The first violation of LGI in a three-level system was reported by George *et al.* They implemented their experiment under the LSUR in a nitrogen-vacancy center in diamond system [16]. In 2017, the first three-level experiment that tested the LGI under the VSUR was realized in the nuclear magnetic resonance system [17]. In the same year, the violation of three-dimensional LGI under the VSUR was realized in the single-photon system [18]. In 2022, Maimaitiyiming *et al.* used a three-level system to test the LGI under the VSUR in a nitrogen-vacancy center in diamond system [19]. However, they only collected one data point, and the experimental value is not very consistent with the ideal theoretical value subject to the short coherence time of this system. Moreover, all the experiments in three-level systems mentioned above only adopted one state update rule and did not give a direct comparison of  $K_3$  under two state update rules experimentally.

In this work, we experimentally test the LGI in a three-level trapped-ion system under the evolution model of a large spin precessing in a magnetic field [4]. Under this model, we obtained a significant violation in a three-level system benefiting from the high-fidelity operations and long coherence time of

\*These authors contributed equally to this work.

†weiwu@nudt.edu.cn

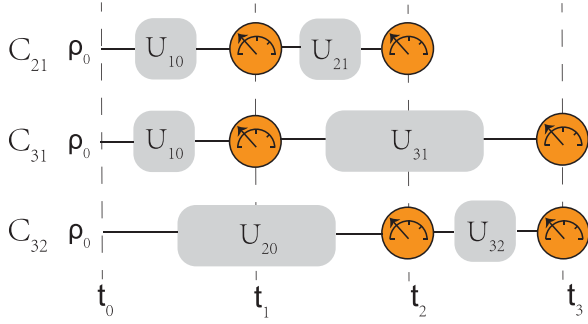


FIG. 1. Scheme for the LGI test.  $\rho_0$  represents the initial density operator. Three separate experiments need to be performed to obtain  $C_{21}$ ,  $C_{32}$ , and  $C_{31}$ . The  $Q$  values are measured at the corresponding two moments, and each experiment is performed multiple times to obtain the joint probability  $P_{ij}(Q_i, Q_j)$ .

the trapped-ion system. Moreover, the VSUR and LSUR are employed in LGI research for direct experimental comparative analysis. Our results show different upper bounds of LGI under two state update rules.

## II. THEORETICAL MODEL

LGI considers the temporal correlation of system evolution. We can assume that there exists a dichotomous observable quantity  $Q = \pm 1$  in a macroscopic system. Due to the MR assumption, a system's state can only take a definite ontic state corresponding to  $Q = +1$  or  $Q = -1$ . The correlation function between moments  $t_i$  and  $t_j$  is

$$C_{ij} = \sum_{Q_i, Q_j = \pm 1} Q_i Q_j P_{ij}(Q_i, Q_j), \quad (2)$$

where  $P_{ij}(Q_i, Q_j)$  represents the joint probability of obtaining the measurement outcomes  $Q_i$  and  $Q_j$  at moments  $t_i$  and  $t_j$ . Three correlation functions  $C_{21}$ ,  $C_{31}$ , and  $C_{32}$  can be defined by selecting three measurement moments  $t_1$ ,  $t_2$ , and  $t_3$ , and then we can define

$$K_3 = C_{21} + C_{32} - C_{31}. \quad (3)$$

Under the restriction of the NIM assumption, it is easy to derive Eq. (1) [20]. The measurement of  $K_3$  requires three independent experiments, and each experiment selects two of the three measurement moments to obtain  $C_{21}$ ,  $C_{32}$ , and  $C_{31}$ . The experimental process is shown in Fig. 1.

A quantum system can violate the LGI, and the maximum value of  $K_3$  is 1.5 in a two-dimensional quantum system. Regarding systems with three or more dimensions, the maximum value of  $K_3$  depends on the state update rule. According to the LSUR, the state after measurement updates following

$$\rho_L \mapsto \Pi_{\pm} \rho \Pi_{\pm}, \quad (4)$$

where  $\Pi_+$  and  $\Pi_-$  denote projection operators corresponding to  $+1$  and  $-1$ , respectively [4]. Under the VSUR, the state updates following

$$\rho_V \mapsto \sum_k (\Pi_{\pm}^k \rho \Pi_{\pm}^k), \quad (5)$$

where  $\Pi_{\pm}^k$  denote one-dimensional projection operators and  $k$  denotes the degeneracy of eigenvalue  $Q$  [4]. It is easy to see that the measurement under the LSUR only distinguishes eigenspaces corresponding to different eigenvalues but does not distinguish which one-dimensional subspace is projected to. However, the measurement using the VSUR projects each one-dimensional subspace and obtains more information. Therefore, the LSUR respects degeneracy, but the VSUR destroys degeneracy. The maximum value of  $K_3$  is 1.5 and is independent of the system's dimension under the LSUR, but it can exceed 1.5 when the VSUR is adopted. Some works claim that this transcendental behavior comes from the fact that the VSUR introduces an additional nonclassicality and cannot be considered a violation of macrorealism in the usual sense [21].

In this work, we employ the model of a large spin precessing in a magnetic field mentioned in Ref. [4] in a three-level system. The corresponding Hamiltonian ( $\hbar = 1$ ) can be expressed as

$$H = \Omega J_x, \quad (6)$$

where  $\Omega$  is the level spacing and  $J_x$  is the  $x$  component of the angular momentum operator. The correlation function between two moments  $t_{\alpha}$  and  $t_{\beta}$  can be written as

$$C_{\beta\alpha} = \sum_{l,m} q_l q_m \text{Tr}\{\Pi_m U_{\beta\alpha} \Pi_l U_{\alpha 0} \rho_0 U_{\alpha 0}^{\dagger} \Pi_l U_{\beta\alpha}^{\dagger}\}, \quad (7)$$

where  $q_l$  and  $q_m$  denote the output results  $\pm 1$  related to the projection operators  $\Pi_l$  and  $\Pi_m$ , respectively [4]. The VSUR is adopted when  $\Pi_l$  and  $\Pi_m$  represent a one-dimensional projection operator, and the LSUR is adopted when  $\Pi_l$  and  $\Pi_m$  represent the projection operator of the eigenspace corresponding to a certain eigenvalue.  $\rho_0$  denotes the density operator at the initial moment  $t_0$ .  $U_{\beta\alpha}$  denotes the unitary evolution operator between the moments  $t_{\alpha}$  and  $t_{\beta}$ , which can be written as

$$U_{\beta\alpha} = e^{-iH(t_{\beta}-t_{\alpha})}. \quad (8)$$

We define three measurement moments  $t_1$ ,  $t_2$ , and  $t_3$ , and set the time intervals as

$$\Omega(t_1 - t_0) = \pi; \quad (9)$$

$$t_2 - t_1 = t_3 - t_2 = \tau. \quad (10)$$

According to our experimental settings under the LSUR,  $K_3$  reads

$$K_3 = -\frac{1}{8} + 2 \cos(\Omega\tau) - \cos(2\Omega\tau) + \frac{1}{8} \cos(4\Omega\tau). \quad (11)$$

Under the VSUR,  $K_3$  reads

$$K_3 = \frac{1}{16} + 2 \cos(\Omega\tau) - \frac{5}{4} \cos(2\Omega\tau) + \frac{3}{16} \cos(4\Omega\tau). \quad (12)$$

We measure the magnitude of  $K_3$  under different values of  $\Omega\tau \in [0, 2\pi]$ .

In the trapped-ion system, we use the laser-ion interaction to control the ion qutrit. An ion with an energy level spacing  $\omega_0$ , interacting with a laser of the frequency  $\omega_l$  forms a system, and the Hamiltonian reads

$$H_L = H_0 + H_I, \quad (13)$$

where  $H_0$  describes the energy of the ion itself and  $H_I$  describes the laser-ion interaction. The coupling strength is given by Rabi frequency  $\Omega_R$ .  $H_0$  and  $H_I$  can be expressed as

$$H_0 = \frac{1}{2} \hbar \omega_0 \sigma_z \quad (14)$$

and

$$H_I = \frac{1}{2} \hbar \Omega_R (\sigma^+ + \sigma^-) (e^{i(\omega_l t + \phi)} + e^{-i(\omega_l t + \phi)}). \quad (15)$$

Here,  $\phi$  denotes the initial phase of the laser,  $t$  denotes the duration of interaction between the laser and the ion,  $\sigma_z$  denotes the  $z$  component of the Pauli operator, and  $\sigma^+$  ( $\sigma^-$ ) is the spin-flip operator. In the rotating frame with  $\omega_0 = \omega_l$ , the interaction Hamiltonian can be written as

$$H_I = \frac{1}{2} \hbar \Omega_R (e^{i\phi} \sigma^+ + e^{-i\phi} \sigma^-). \quad (16)$$

The evolution operator under  $H_I$  is the rotation operation in a two-dimensional Hilbert space

$$R(\theta, \phi) = \begin{pmatrix} \cos \frac{\theta}{2} & -i \sin \frac{\theta}{2} e^{-i\phi} \\ -i \sin \frac{\theta}{2} e^{i\phi} & \cos \frac{\theta}{2} \end{pmatrix}, \quad (17)$$

where  $\theta$  and  $\phi$  denote the angle and phase of the rotation operation. All operations in the experiment must formally satisfy Eq. (17). For example, two-dimensional rotations in

$$U_{10} = \begin{pmatrix} 0 & 0 & -1 & 0 \\ 0 & -1 & 0 & 0 \\ -1 & 0 & 0 & 0 \\ 0 & 0 & 0 & 1 \end{pmatrix} = \begin{pmatrix} 1 & 0 & 0 & 0 \\ 0 & 1 & 0 & 0 \\ 0 & 0 & -1 & 0 \\ 0 & 0 & 0 & -1 \end{pmatrix} \begin{pmatrix} 0 & 0 & -1 & 0 \\ 0 & 1 & 0 & 0 \\ 1 & 0 & 0 & 0 \\ 0 & 0 & 0 & 1 \end{pmatrix} \begin{pmatrix} 1 & 0 & 0 & 0 \\ 0 & -1 & 0 & 0 \\ 0 & 0 & 1 & 0 \\ 0 & 0 & 0 & -1 \end{pmatrix}. \quad (20)$$

If the evolution time does not satisfy  $\Omega(t_\beta - t_\alpha) = \pi$ , the high-dimensional matrix needs to be decomposed according to the method given in Ref. [22] (see Appendix A for a detailed decomposition process).

### III. EXPERIMENTAL SETUP AND RESULTS ANALYSIS

In this work, the LGI test is demonstrated using a single  $^{40}\text{Ca}^+$  ion trapped in a blade linear Paul trap [23]. The ion needs to be cooled first. The cooling schemes used in our experiment include Doppler cooling [24], electromagnetically induced transparency (EIT) cooling [25–27], and sideband cooling [24]. After the whole cooling process, the mean phonon number of the ion can be brought down below 0.1. In addition, we trigger the experimental sequence synchronized to the 50-Hz frequency to prevent noise from the power supply [28].

the three-dimensional space can be represented as Eqs. (18) and (19),

$$R_1(\theta_1, \phi_1) = \begin{pmatrix} \cos \frac{\theta_1}{2} & -i \sin \frac{\theta_1}{2} e^{-i\phi_1} & 0 \\ -i \sin \frac{\theta_1}{2} e^{i\phi_1} & \cos \frac{\theta_1}{2} & 0 \\ 0 & 0 & 1 \end{pmatrix}, \quad (18)$$

$$R_2(\theta_2, \phi_2) = \begin{pmatrix} \cos \frac{\theta_2}{2} & 0 & -i \sin \frac{\theta_2}{2} e^{-i\phi_2} \\ 0 & 1 & 0 \\ -i \sin \frac{\theta_2}{2} e^{i\phi_2} & 0 & \cos \frac{\theta_2}{2} \end{pmatrix}. \quad (19)$$

For three-dimensional unitary evolution, we need to decompose it into two-dimensional evolution with this form. We also need to convert the two-dimensional matrix that does not conform to the form of Eq. (17) into this form. A unitary matrix which acts on a high-dimensional Hilbert space can be decomposed into a product of two-level rotation matrices which act nontrivially only on two vector components [22]. To facilitate the decomposition process of the three-dimensional unitary matrix, we introduce an auxiliary dimension in our experiment, defined as the fourth dimension in the matrix. According to the general method mentioned in Ref. [22], we decompose the three-dimensional matrix into the product of two-dimensional matrices. But some two-dimensional matrices differ by a  $\pi$  phase in one dimension from the form shown in Eq. (17). The auxiliary energy level is employed to eliminate this  $\pi$  phase so that the two-dimensional matrix conforms to the form shown in Eq. (17). Equations (A6) and (A7) in Appendix A give examples of its application.

If the system's evolution time satisfies  $\Omega(t_\beta - t_\alpha) = \pi$ , the original three-dimensional evolution operator, via expanding to four-dimensional Hilbert space, can be decomposed into the product of three matrices as

$$\begin{pmatrix} 0 & 0 & -1 & 0 \\ 0 & -1 & 0 & 0 \\ 0 & 0 & 0 & -1 \\ -1 & 0 & 0 & 0 \end{pmatrix} \begin{pmatrix} 0 & 0 & -1 & 0 \\ 0 & 1 & 0 & 0 \\ 1 & 0 & 0 & 0 \\ 0 & 0 & 0 & 1 \end{pmatrix} \begin{pmatrix} 1 & 0 & 0 & 0 \\ 0 & -1 & 0 & 0 \\ 0 & 0 & 1 & 0 \\ 0 & 0 & 0 & -1 \end{pmatrix}. \quad (20)$$

The energy levels of  $^{40}\text{Ca}^+$  have fine structure splitting under the magnetic field, as shown in Fig. 2. We construct a qutrit using three levels of  $|0\rangle = |4S_{1/2}(m_J = -1/2)\rangle$ ,  $|1\rangle = |3D_{5/2}(m_J = -1/2)\rangle$ , and  $|2\rangle = |3D_{5/2}(m_J = +1/2)\rangle$ , and set the lowest energy level  $|0\rangle$  as the initial state of our experiment. We select  $|aux\rangle = |4S_{1/2}(m_J = +1/2)\rangle$  as the auxiliary energy level. We define  $Q = -1$  when the ion is in state  $|0\rangle$  and  $Q = +1$  when the ion is in state  $|1\rangle$  or  $|2\rangle$ .

The transition  $4S_{1/2} \leftrightarrow 3D_{5/2}$  involved in our experiment is controlled by a 729-nm light provided by the Ti:sapphire laser. The laser's frequency, phase, amplitude, and duration are controlled by an arbitrary waveform generator (AWG) via an acousto-optic modulator (AOM). We calibrate the transition frequencies and  $\Omega_R$  of the four spectral lines  $4S_{1/2}(m_J = \pm 1/2) \leftrightarrow 3D_{5/2}(m_J = \pm 1/2)$  by scanning laser frequency and duration. According to the specific  $\tau$ , we can determine the specific form of the evolution operators  $U_{\beta\alpha}$  by Eq. (8).

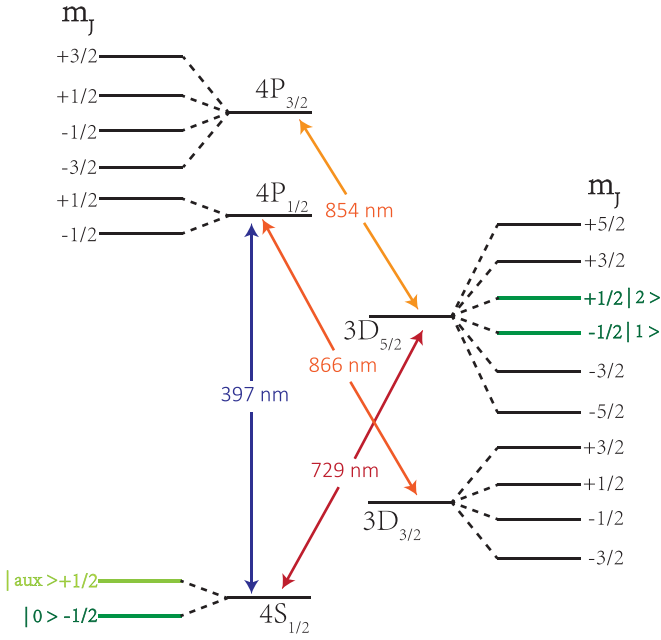


FIG. 2. Energy level diagram of  $^{40}\text{Ca}^+$ . The three levels  $4S_{1/2}(m_J = -1/2)$ ,  $3D_{5/2}(m_J = -1/2)$ , and  $3D_{5/2}(m_J = +1/2)$  form a qutrit and  $4S_{1/2}(m_J = +1/2)$  is the auxiliary energy level.

A set of  $R(\theta, \phi)$  can be obtained by matrix decomposition of the evolution operator. In the rotation operation  $R(\theta, \phi)$ ,  $\theta$  is related to the laser duration, which can be determined by

$$t = \frac{\theta}{\Omega_R}, \quad (21)$$

and  $\phi$  denotes the relative phase of the laser that can be set directly by the AWG. According to the Pound-Drever-Hall (PDH) error signal spectrum measured by a rf spectrum analyzer, the phase noise has been proved to be from the specific frequency band of the Ti:sapphire laser [27]. To avoid the ac Stark frequency shift under the high power laser and the noise mentioned above, we select  $\Omega_R$  at about  $2\pi \times 8\text{ kHz}$  in our experiment. The  $3D_{5/2}$  level has a long lifetime. The ion needs to be quickly initialized to the ground state by using an 854-nm laser during the sideband cooling process and after the quantum state manipulation. The specific method is to use the 854-nm laser to make the ion transition from the  $3D_{5/2}$  level to the short-lived  $4P_{3/2}$  level, after which the ion will rapidly decay to the ground energy level spontaneously.

The electron shelving technique [29–31] is used to discriminate between state  $|0\rangle$  and state  $|1\rangle$  or  $|2\rangle$ . State  $|0\rangle$  is detected when the photomultiplier (PMT) collects the fluorescence. No fluorescence can be observed if the ion is in state  $|1\rangle$  or  $|2\rangle$ , as the  $D_{5/2}$  level is not coupled to the  $P_{1/2}$  level by the 397-nm laser. Since the ion in the  $P_{1/2}$  level has a probability of leaking to the  $D_{3/2}$  level, an 866-nm laser is needed to pump the ion back to the  $S_{1/2} \leftrightarrow P_{1/2}$  transition cycle. In the LGI test under the LSUR, we define Q as 1 when the ion is in state  $|1\rangle$  or  $|2\rangle$ , so we only need to distinguish state  $|0\rangle$  and state  $|1\rangle$  or  $|2\rangle$  by the electron shelving technique as shown in Fig. 3(a). However, in the LGI test under the VSUR, we need to determine whether the ion is located in state  $|0\rangle$ , state  $|1\rangle$ , or state  $|2\rangle$ . The sequence of four-step operations of the measurement

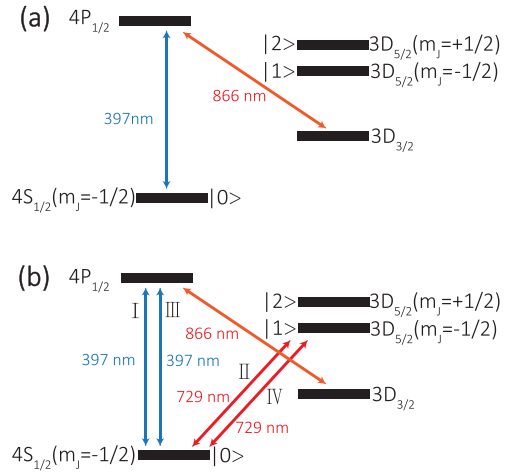


FIG. 3. Schemes for two different measurement methods. (a) The measurement scheme using the LSUR. (b) The measurement scheme using the VSUR. The laser sequence used in the four-step operations of the measurement is shown by serial numbers I, II, III, and IV.

is shown by serial numbers I, II, III, and IV in Fig. 3(b). We first distinguish whether the ion is in state  $|0\rangle$  by the electron shelving technique. Secondly, we exchange state  $|0\rangle$  and state  $|1\rangle$  with the 729-nm laser. Then, we determine whether the ion is in state  $|0\rangle$  at this time. If so, the ion is in state  $|1\rangle$  before the state exchange; otherwise, it is in state  $|2\rangle$  before the state exchange. Finally, if the measurement is carried out before the second unitary evolution, we need to use the identical 729-nm laser to make the state of the ion return to the state before step II for the second unitary evolution by applying step IV. We discuss the effects of additional energy levels and the reliability of this measurement method in Appendix B. After the electron shelving process, the ion will be heated and may spontaneously decay to the  $4S_{1/2}(m_J = +1/2)$  level. We use EIT cooling after each electron shelving process to suppress the heating effect. We use optical pumping to ensure the ion returns to the  $4S_{1/2}(m_J = -1/2)$  level.

Each set of experiments is repeated at least 10 000 times to obtain the populations of ion state. According to the populations, we can calculate  $C_{\beta\alpha}$ , and then get  $K_3$  by Eq. (1). The values of  $K_3$  corresponding to different  $\Omega\tau$  are shown in Fig. 4. Figures 4(a) and 4(b) are the experimental results under the LSUR and VSUR, respectively. The black curve is the theoretical result, the red dots are experimental results, the orange horizontal line is the CB, and the violet horizontal line is the LB. It can be seen that  $K_3$  exceeds the CB regardless of which state update rule is used. It is not surprising that the LGI is violated, as the state of a single ion definitely can be superposition. Under the same experimental settings, we discover that the  $K_3$  does not exceed the LB under the LSUR, but it exceeds the LB under the VSUR. Under the VSUR, the theoretical maximum value is 1.7565, appearing at about  $\Omega\tau = 1.585\pi$ . The maximum value in our experiment is  $1.739 \pm 0.014$ , appearing at  $\Omega\tau = 1.6\pi$ , which exceeds the LB with a  $17\sigma$  confidence level, and agrees with the theoretical value at  $\Omega\tau = 1.6\pi$ , which is 1.750. The difference of LGI's upper bound is related to the projection measurement protocol of two state update rules. The projection measurement

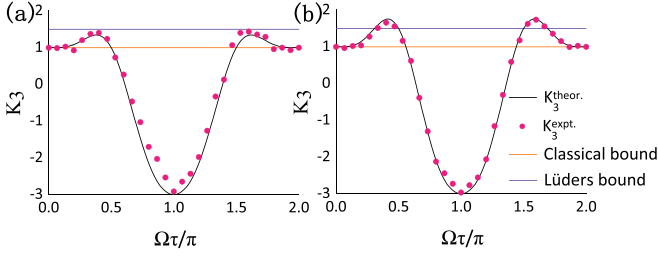


FIG. 4. Experimental results of  $K_3$  under 31 different settings of  $\Omega\tau \in [0, 2\pi]$ . (a) The experimentally determined result under the LSUR. (b) The experimentally determined result under the VSUR. The black curve is the theoretical result, the red dots are the experimental results, the orange horizontal line is the classical bound, and the violet horizontal line is the Lüders bound. The error bars are not visible as the statistical error is about  $10^{-2}$ .

protocol under the VSUR measures each one-dimensional space, which makes the wave function collapse completely, but the projection measurement protocol under the LSUR retains the coherence between states  $|1\rangle$  and  $|2\rangle$ . When the eigenvalue  $Q = -1$ , there is no difference between the projection measurement protocol under the LSUR and VSUR because there is no degeneracy. However, the situation is different when the eigenvalue  $Q = +1$ .  $\Pi_1$  and  $\Pi_2$  project the ion state to states  $|1\rangle$  and  $|2\rangle$ , respectively. According to the LSUR, after one measurement, the change of the density operator can be described as

$$\begin{aligned} \rho_L &= \Pi_+ \rho_0 \Pi_+ = (\Pi_1 + \Pi_2) \rho_0 (\Pi_1 + \Pi_2) \\ &= \Pi_1 \rho_0 \Pi_1 + \Pi_2 \rho_0 \Pi_2 + \Pi_1 \rho_0 \Pi_2 + \Pi_2 \rho_0 \Pi_1. \end{aligned} \quad (22)$$

However, the change of the density operator under the VSUR is described as

$$\begin{aligned} \rho_V &= \Pi_1 \rho_0 \Pi_1 + \Pi_2 \rho_0 \Pi_2 \\ &= \rho_L - (\Pi_1 \rho_0 \Pi_2 + \Pi_2 \rho_0 \Pi_1). \end{aligned} \quad (23)$$

The term  $-(\Pi_1 \rho_0 \Pi_2 + \Pi_2 \rho_0 \Pi_1)$  is responsible for the violation of the LB.

The experimental error in our LGI test mainly comes from the following four factors. Firstly, the decoherence of the ion contributes to the deviation between theoretical and experimental results. It is worth mentioning that the measurement under the VSUR has more experimental steps but the experimental results under the VSUR are more consistent with the theory. Unlike the measurement protocol under the VSUR, the measurement under the LSUR retains the coherence between states  $|1\rangle$  and  $|2\rangle$ , so the coherence time has more effect on the measurement under the LSUR. Secondly, according to data from the experimental calibration process, the fidelity of the evolution operations is slightly worse at low power of the 729-nm laser. There will be a large ac Stark frequency shift when the 729-nm laser power is high; on the other hand, the

phase noise will increase with the decrease of the laser power due to the locking circuit of this narrow line-width laser. The ac Stark frequency shift will affect the energy level spacing in our experiment, and the phase noise will affect the purity of the 729-nm laser. To trade off the influence of the ac Stark frequency shift and the phase noise, we choose the appropriate laser power.  $\Omega_R$  of four spectral lines in our experiment are about  $2\pi \times 8$  kHz. Under this  $\Omega_R$ , the influence of the ac Stark frequency shift can be almost ignored, and the average evolution fidelity is about 98%. There are two main influences of the evolution infidelity. One is that the ion is not evolved according to the expected probability distribution after the operation of the laser pulse, and the error is accumulated after the operation of multiple imperfect laser pulses. The second influence comes from the auxiliary energy level. During the actual experiment, the auxiliary energy level involved in the evolution has a small residual probability, which will increase the probability that the ion is in state  $|0\rangle$ . However, all the evolved pulses involved in the auxiliary energy level are  $2\pi$  pulses, and the fidelity of  $2\pi$  pulses will be significantly higher than other non- $\pi$  integer times pulses, so the probability of electrons remaining in the auxiliary energy level is rather small and has no great influence on our experimental results and the conclusion. Thirdly, the fidelity of our initial state preparation is about 99.4% because the polarization of the laser is not pure, and it is difficult to make the laser absolutely parallel with the magnetic field. Fourthly, during this period of our experiment, the power of the 397-nm laser slightly fluctuates. Since the electron shelving technique is implemented by a 397-nm laser, the fluctuation may slightly affect the measurement fidelity, and the 397-nm laser instability affects the effect of Doppler cooling too.

#### IV. CONCLUSION

We have realized the LGI test in a three-level trapped-ion system, and obtained  $K_3$  under the LSUR and the VSUR, respectively, which are consistent with the theoretical predictions. We directly compared the upper bound of LGI under two state update rules in the same experimental system. We adopted the model of a large spin precession in the magnetic field, and experimentally obtained a significant violation under the VSUR, which benefits from the high-fidelity operations and long coherence time of the trapped-ion system.

#### ACKNOWLEDGMENTS

This work is supported by the National Natural Science Foundation of China under Grants No. 12174447, No. 11904402, No. 12004430, No. 12074433, No. 12174448, and No. 12204543, the Innovation Program for Quantum Science and Technology No. 2021ZD0301605, and the Science and Technology Innovation Program of Hunan Province under Grant No. 2022RC1194.

#### APPENDIX A: THE MATRIX DECOMPOSITION

The corresponding relationship between the energy levels and the elements  $M_{qp}$  of the four-dimensional matrix is shown in Table I. Three experimental levels,  $4S_{1/2}(m_J = -1/2)$ ,  $3D_{5/2}(m_J = -1/2)$ ,  $3D_{5/2}(m_J = +1/2)$ , and an auxiliary  $4S_{1/2}(m_J = +1/2)$  energy level correspond to the first, second, third, and fourth dimension of the matrix, respectively.

TABLE I. The corresponding relationship between the energy levels and matrix elements  $M_{qp}$ .

	$4S_{1/2}(m_J = -1/2)$	$3D_{5/2}(m_J = -1/2)$	$3D_{5/2}(m_J = +1/2)$	$4S_{1/2}(m_J = +1/2)$
$4S_{1/2}(m_J = -1/2)$	$M_{11}$	$M_{12}$	$M_{13}$	$M_{14}$
$3D_{5/2}(m_J = -1/2)$	$M_{21}$	$M_{22}$	$M_{23}$	$M_{24}$
$3D_{5/2}(m_J = +1/2)$	$M_{31}$	$M_{32}$	$M_{33}$	$M_{34}$
$4S_{1/2}(m_J = +1/2)$	$M_{41}$	$M_{42}$	$M_{43}$	$M_{44}$

The  $x$  component of the spin angular momentum in the three-dimensional space is

$$J_x = \frac{1}{\sqrt{2}} \begin{pmatrix} 0 & 1 & 0 \\ 1 & 0 & 1 \\ 0 & 1 & 0 \end{pmatrix}. \quad (\text{A1})$$

When  $\Omega(t_\beta - t_\alpha) \neq \pi$ , let  $\Omega\tau = \epsilon$ , then the unitary evolution operator can be written as

$$U_{\beta\alpha} = e^{-iH(t_\beta - t_\alpha)} = e^{-iJ_x\Omega(t_\beta - t_\alpha)} = e^{-iJ_x\epsilon} = \begin{pmatrix} \frac{1}{2} + \frac{\cos\epsilon}{2} & \frac{-i\sin\epsilon}{\sqrt{2}} & -\frac{1}{2} + \frac{\cos\epsilon}{2} \\ \frac{-i\sin\epsilon}{\sqrt{2}} & \cos\epsilon & \frac{-i\sin\epsilon}{\sqrt{2}} \\ -\frac{1}{2} + \frac{\cos\epsilon}{2} & \frac{-i\sin\epsilon}{\sqrt{2}} & \frac{1}{2} + \frac{\cos\epsilon}{2} \end{pmatrix}. \quad (\text{A2})$$

According to the method in Ref. [22],  $U_{\beta\alpha}$  can be decomposed into

$$U_{\beta\alpha} = \begin{pmatrix} \frac{\sqrt{2}(1+\cos\epsilon)}{\sqrt{5+4\cos\epsilon-\cos 2\epsilon}} & \frac{2i\sin\epsilon}{\sqrt{5+4\cos\epsilon-\cos 2\epsilon}} & 0 \\ -\frac{2i\sin\epsilon}{\sqrt{5+4\cos\epsilon-\cos 2\epsilon}} & -\frac{\sqrt{2}(1+\cos\epsilon)}{\sqrt{5+4\cos\epsilon-\cos 2\epsilon}} & 0 \\ 0 & 0 & 1 \end{pmatrix} \begin{pmatrix} \frac{\cos^2 \frac{\epsilon}{2} \sqrt{3-\cos\epsilon}}{\sqrt{2}|\cos \frac{\epsilon}{2}|} & 0 & \frac{1}{2}(-1+\cos\epsilon) \\ 0 & 1 & 0 \\ \frac{1}{2}(-1+\cos\epsilon) & 0 & -\frac{\cos^2 \frac{\epsilon}{2} \sqrt{3-\cos\epsilon}}{\sqrt{2}|\cos \frac{\epsilon}{2}|} \end{pmatrix} \\ \times \begin{pmatrix} 1 & 0 & 0 \\ 0 & \frac{-1-\cos\epsilon}{|\cos \frac{\epsilon}{2}| \sqrt{6-2\cos\epsilon}} & \frac{2i\sin\epsilon}{\sqrt{5+4\cos\epsilon-\cos 2\epsilon}} \\ 0 & \frac{2i\sin\epsilon}{\sqrt{5+4\cos\epsilon-\cos 2\epsilon}} & \frac{-1-\cos\epsilon}{|\cos \frac{\epsilon}{2}| \sqrt{6-2\cos\epsilon}} \end{pmatrix}. \quad (\text{A3})$$

In Sec. II, we have derived that only matrices in the form of Eq. (17) can be realized in the trapped-ion system, and its form is

$$R(\theta, \varphi) = \begin{pmatrix} \cos \frac{\theta}{2} & -i \sin \frac{\theta}{2} e^{-i\varphi} \\ -i \sin \frac{\theta}{2} e^{i\varphi} & \cos \frac{\theta}{2} \end{pmatrix}. \quad (\text{A4})$$

We note that the forms of the matrices in Eq. (A3) are different from Eq. (A4). We first expand the three matrices in Eq. (A3) from three-dimensional to four-dimensional:

$$U_{\beta\alpha} = \begin{pmatrix} \frac{\sqrt{2}(1+\cos\epsilon)}{\sqrt{5+4\cos\epsilon-\cos 2\epsilon}} & \frac{2i\sin\epsilon}{\sqrt{5+4\cos\epsilon-\cos 2\epsilon}} & 0 & 0 \\ -\frac{2i\sin\epsilon}{\sqrt{5+4\cos\epsilon-\cos 2\epsilon}} & -\frac{\sqrt{2}(1+\cos\epsilon)}{\sqrt{5+4\cos\epsilon-\cos 2\epsilon}} & 0 & 0 \\ 0 & 0 & 1 & 0 \\ 0 & 0 & 0 & 1 \end{pmatrix} \\ \times \begin{pmatrix} \frac{\cos^2 \frac{\epsilon}{2} \sqrt{3-\cos\epsilon}}{\sqrt{2}|\cos \frac{\epsilon}{2}|} & 0 & \frac{1}{2}(-1+\cos\epsilon) & 0 \\ 0 & 1 & 0 & 0 \\ \frac{1}{2}(-1+\cos\epsilon) & 0 & -\frac{\cos^2 \frac{\epsilon}{2} \sqrt{3-\cos\epsilon}}{\sqrt{2}|\cos \frac{\epsilon}{2}|} & 0 \\ 0 & 0 & 0 & 1 \end{pmatrix} \begin{pmatrix} 1 & 0 & 0 & 0 \\ 0 & \frac{-1-\cos\epsilon}{|\cos \frac{\epsilon}{2}| \sqrt{6-2\cos\epsilon}} & \frac{2i\sin\epsilon}{\sqrt{5+4\cos\epsilon-\cos 2\epsilon}} & 0 \\ 0 & \frac{2i\sin\epsilon}{\sqrt{5+4\cos\epsilon-\cos 2\epsilon}} & \frac{-1-\cos\epsilon}{|\cos \frac{\epsilon}{2}| \sqrt{6-2\cos\epsilon}} & 0 \\ 0 & 0 & 0 & 1 \end{pmatrix}. \quad (\text{A5})$$

Observe the form of Eq. (A4), where the positive and negative signs of the diagonal elements are the same, and the positive and negative signs of the antidiagonal elements can be the same or the opposite. For the first matrix in Eq. (A5), which does not meet

this requirement, we can transform it into

$$\begin{pmatrix} \frac{\sqrt{2}(1+\cos\epsilon)}{\sqrt{5+4\cos\epsilon-\cos 2\epsilon}} & \frac{2i\sin\epsilon}{\sqrt{5+4\cos\epsilon-\cos 2\epsilon}} & 0 & 0 \\ -\frac{2i\sin\epsilon}{\sqrt{5+4\cos\epsilon-\cos 2\epsilon}} & -\frac{\sqrt{2}(1+\cos\epsilon)}{\sqrt{5+4\cos\epsilon-\cos 2\epsilon}} & 0 & 0 \\ 0 & 0 & 1 & 0 \\ 0 & 0 & 0 & 1 \end{pmatrix} = \begin{pmatrix} 1 & 0 & 0 & 0 \\ 0 & -1 & 0 & 0 \\ 0 & 0 & 1 & 0 \\ 0 & 0 & 0 & -1 \end{pmatrix} \begin{pmatrix} \frac{\sqrt{2}(1+\cos\epsilon)}{\sqrt{5+4\cos\epsilon-\cos 2\epsilon}} & \frac{2i\sin\epsilon}{\sqrt{5+4\cos\epsilon-\cos 2\epsilon}} & 0 & 0 \\ \frac{2i\sin\epsilon}{\sqrt{5+4\cos\epsilon-\cos 2\epsilon}} & \frac{\sqrt{2}(1+\cos\epsilon)}{\sqrt{5+4\cos\epsilon-\cos 2\epsilon}} & 0 & 0 \\ 0 & 0 & 1 & 0 \\ 0 & 0 & 0 & -1 \end{pmatrix}. \tag{A6}$$

Similarly, the second matrix in Eq. (A5) needs a similar transformation:

$$\begin{pmatrix} \frac{\cos^2\frac{\epsilon}{2}\sqrt{3-\cos\epsilon}}{\sqrt{2}|\cos\frac{\epsilon}{2}|} & 0 & \frac{1}{2}(-1+\cos\epsilon) & 0 \\ 0 & 1 & 0 & 0 \\ \frac{1}{2}(-1+\cos\epsilon) & 0 & -\frac{\cos^2\frac{\epsilon}{2}\sqrt{3-\cos\epsilon}}{\sqrt{2}|\cos\frac{\epsilon}{2}|} & 0 \\ 0 & 0 & 0 & 1 \end{pmatrix} = \begin{pmatrix} 1 & 0 & 0 & 0 \\ 0 & 1 & 0 & 0 \\ 0 & 0 & -1 & 0 \\ 0 & 0 & 0 & -1 \end{pmatrix} \begin{pmatrix} \frac{\cos^2\frac{\epsilon}{2}\sqrt{3-\cos\epsilon}}{\sqrt{2}|\cos\frac{\epsilon}{2}|} & 0 & \frac{1}{2}(-1+\cos\epsilon) & 0 \\ 0 & 1 & 0 & 0 \\ -\frac{1}{2}(-1+\cos\epsilon) & 0 & \frac{\cos^2\frac{\epsilon}{2}\sqrt{3-\cos\epsilon}}{\sqrt{2}|\cos\frac{\epsilon}{2}|} & 0 \\ 0 & 0 & 0 & -1 \end{pmatrix}. \tag{A7}$$

The third matrix in Eq. (A5) conforms to the form of Eq. (A4), but it involves an infeasible coupling between  $3D_{5/2}(m_J = -1/2)$  level and  $3D_{5/2}(m_J = +1/2)$  level. We convert it to the coupling of  $4S_{1/2}$  level and  $3D_{5/2}$  level:

$$\begin{pmatrix} 1 & 0 & 0 & 0 \\ 0 & \frac{-1-\cos\epsilon}{|\cos\frac{\epsilon}{2}|\sqrt{6-2\cos\epsilon}} & \frac{2i\sin\epsilon}{\sqrt{5+4\cos\epsilon-\cos 2\epsilon}} & 0 \\ 0 & \frac{2i\sin\epsilon}{\sqrt{5+4\cos\epsilon-\cos 2\epsilon}} & \frac{-1-\cos\epsilon}{|\cos\frac{\epsilon}{2}|\sqrt{6-2\cos\epsilon}} & 0 \\ 0 & 0 & 0 & 1 \end{pmatrix} = \begin{pmatrix} 0 & -1 & 0 & 0 \\ 1 & 0 & 0 & 0 \\ 0 & 0 & 1 & 0 \\ 0 & 0 & 0 & 1 \end{pmatrix} \begin{pmatrix} \frac{-1-\cos\epsilon}{|\cos\frac{\epsilon}{2}|\sqrt{6-2\cos\epsilon}} & 0 & \frac{2i\sin\epsilon}{\sqrt{5+4\cos\epsilon-\cos 2\epsilon}} & 0 \\ 0 & 1 & 0 & 0 \\ \frac{2i\sin\epsilon}{\sqrt{5+4\cos\epsilon-\cos 2\epsilon}} & 0 & \frac{-1-\cos\epsilon}{|\cos\frac{\epsilon}{2}|\sqrt{6-2\cos\epsilon}} & 0 \\ 0 & 0 & 0 & 1 \end{pmatrix} \begin{pmatrix} 0 & 1 & 0 & 0 \\ -1 & 0 & 0 & 0 \\ 0 & 0 & 1 & 0 \\ 0 & 0 & 0 & 1 \end{pmatrix}. \tag{A8}$$

Combining Eqs. (A6), (A7), and (A8), and the matrix element  $M_{44}$  of the second matrix on the right side of the equal sign of the Eqs. (A6) and (A7) can be taken as positive under the premise that the product is unchanged, we finally get

$$U_{\beta\alpha} = \begin{pmatrix} 1 & 0 & 0 & 0 \\ 0 & -1 & 0 & 0 \\ 0 & 0 & 1 & 0 \\ 0 & 0 & 0 & -1 \end{pmatrix} \begin{pmatrix} \frac{\sqrt{2}(1+\cos\epsilon)}{\sqrt{5+4\cos\epsilon-\cos 2\epsilon}} & \frac{2i\sin\epsilon}{\sqrt{5+4\cos\epsilon-\cos 2\epsilon}} & 0 & 0 \\ \frac{2i\sin\epsilon}{\sqrt{5+4\cos\epsilon-\cos 2\epsilon}} & \frac{\sqrt{2}(1+\cos\epsilon)}{\sqrt{5+4\cos\epsilon-\cos 2\epsilon}} & 0 & 0 \\ 0 & 0 & 1 & 0 \\ 0 & 0 & 0 & 1 \end{pmatrix} \begin{pmatrix} 1 & 0 & 0 & 0 \\ 0 & 1 & 0 & 0 \\ 0 & 0 & -1 & 0 \\ 0 & 0 & 0 & -1 \end{pmatrix} \\ \times \begin{pmatrix} \frac{\cos^2\frac{\epsilon}{2}\sqrt{3-\cos\epsilon}}{\sqrt{2}|\cos\frac{\epsilon}{2}|} & 0 & \frac{1}{2}(-1+\cos\epsilon) & 0 \\ 0 & 1 & 0 & 0 \\ -\frac{1}{2}(-1+\cos\epsilon) & 0 & \frac{\cos^2\frac{\epsilon}{2}\sqrt{3-\cos\epsilon}}{\sqrt{2}|\cos\frac{\epsilon}{2}|} & 0 \\ 0 & 0 & 0 & 1 \end{pmatrix} \begin{pmatrix} 0 & -1 & 0 & 0 \\ 1 & 0 & 0 & 0 \\ 0 & 0 & 1 & 0 \\ 0 & 0 & 0 & 1 \end{pmatrix} \begin{pmatrix} \frac{-1-\cos\epsilon}{|\cos\frac{\epsilon}{2}|\sqrt{6-2\cos\epsilon}} & 0 & \frac{2i\sin\epsilon}{\sqrt{5+4\cos\epsilon-\cos 2\epsilon}} & 0 \\ 0 & 1 & 0 & 0 \\ \frac{2i\sin\epsilon}{\sqrt{5+4\cos\epsilon-\cos 2\epsilon}} & 0 & \frac{-1-\cos\epsilon}{|\cos\frac{\epsilon}{2}|\sqrt{6-2\cos\epsilon}} & 0 \\ 0 & 0 & 0 & 1 \end{pmatrix} \\ \times \begin{pmatrix} 0 & 1 & 0 & 0 \\ -1 & 0 & 0 & 0 \\ 0 & 0 & 1 & 0 \\ 0 & 0 & 0 & 1 \end{pmatrix}. \tag{A9}$$

TABLE II. The probability of three states and their sum.

Serial number	Probability in $ 0\rangle$	Probability in $ 1\rangle$	Probability in $ 2\rangle$	Sum
1	94.07%	0.82%	5.06%	99.95%
2	68.20%	3.73%	27.88%	99.81%
3	34.91%	12.01%	52.66%	99.58%
4	7.38%	49.53%	42.66%	99.57%
5	2.51%	69.63%	27.58%	99.72%
6	1.94%	92.82%	4.85%	99.61%

## APPENDIX B: DISCUSSION ON MEASUREMENT METHOD UNDER THE VSUR

We prepared the initial state of the ion in state  $|0\rangle$  and randomly selected some unitary evolutions to control the ion state. Then we measured the three states of  $|0\rangle$ ,  $|1\rangle$ , and  $|2\rangle$ , respectively. The specific measurement process is to measure

state  $|0\rangle$  first, then we exchange state  $|0\rangle$  with state  $|1\rangle$  and measure whether the ion is in the  $4S_{1/2}(m_J = -1/2)$  level. Next, we exchange state  $|0\rangle$  this moment with state  $|2\rangle$  and measure whether the ion is in the  $4S_{1/2}(m_J = -1/2)$  level. The experiment was repeated 10 000 times to obtain the probabilities of the ion being in states  $|0\rangle$ ,  $|1\rangle$ , and  $|2\rangle$ , respectively. The probabilities were added together to see if their sum was 100%. Our experimental results are shown in Table II.

Table II shows that the sum of the probabilities of the three states is above 99.5%. In this experiment, there are two state exchange processes. The fidelity of each state exchange process is about 99.5%, so the overall fidelity of the two state exchange processes is about 99%. Therefore, our measurement results are within the measurement error allowed by the evolution fidelity. This result can be explained as follows: In our experiment, the energy level spacing between adjacent Zeeman levels is about  $2\pi \times 4.4$  MHz, and the Rabi frequency is about  $2\pi \times 8$  kHz, so the probability of nonresonant transition is almost zero.

- 
- [1] R. J. Glauber, The quantum theory of optical coherence, *Phys. Rev.* **130**, 2529 (1963).
- [2] E. Schrödinger, Die gegenwärtige situation in der quantenmechanik, *Naturwissenschaften* **23**, 844 (1935).
- [3] A. J. Leggett and A. Garg, Quantum Mechanics Versus Macroscopic Realism: Is the Flux There when Nobody Looks?, *Phys. Rev. Lett.* **54**, 857 (1985).
- [4] C. Budroni and C. Emary, Temporal Quantum Correlations and Leggett-Garg Inequalities in Multilevel Systems, *Phys. Rev. Lett.* **113**, 050401 (2014).
- [5] B. S. Cirel'son, Quantum generalizations of Bell's inequality, *Lett. Math. Phys.* **4**, 93 (1980).
- [6] H. S. Poh, S. K. Joshi, A. Cere, A. Cabello, and C. Kurtsiefer, Approaching Tsirelson's Bound in a Photon Pair Experiment, *Phys. Rev. Lett.* **115**, 180408 (2015).
- [7] M. Navascués, S. Pironio, and A. Acín, A convergent hierarchy of semidefinite programs characterizing the set of quantum correlations, *New J. Phys.* **10**, 073013 (2008).
- [8] C. Budroni, T. Moroder, M. Kleinmann, and O. Gühne, Bounding Temporal Quantum Correlations, *Phys. Rev. Lett.* **111**, 020403 (2013).
- [9] G. Lüders, Concerning the state-change due to the measurement process, *Ann. Phys.* **518**, 663 (2006).
- [10] J. Von Neumann, *Mathematical Foundations of Quantum Mechanics: New Edition* (Princeton University Press, Princeton, 2018).
- [11] A. Palacios-Laloy, F. Mallet, F. Nguyen, P. Bertet, D. Vion, D. Esteve, and A. N. Korotkov, Experimental violation of a Bell's inequality in time with weak measurement, *Nat. Phys.* **6**, 442 (2010).
- [12] J. Xu, C. Li, X. Zou, and G. Guo, Experimental violation of the Leggett-Garg inequality under decoherence, *Sci. Rep.* **1**, 101 (2011).
- [13] G. C. Knee, S. Simmons, E. M. Gauger, J. J. L. Morton, H. Riemann, N. V. Abrosimov, P. Becker, H.-J. Pohl, K. M. Itoh, M. L. W. Thewalt *et al.*, Violation of a Leggett-Garg inequality with ideal non-invasive measurements, *Nat. Commun.* **3**, 606 (2012).
- [14] H. Katiyar, A. Shukla, K. R. Koteswara Rao, and T. S. Mahesh, Violation of entropic Leggett-Garg inequality in nuclear spins, *Phys. Rev. A* **87**, 052102 (2013).
- [15] A. Santini and V. Vitale, Experimental violations of Leggett-Garg inequalities on a quantum computer, *Phys. Rev. A* **105**, 032610 (2022).
- [16] R. E. George, L. M. Robledo, O. J. E. Maroney, M. S. Blok, H. Bernien, M. L. Markham, D. J. Twitchen, J. J. L. Morton, G. A. D. Briggs, and R. Hanson, Opening up three quantum boxes causes classically undetectable wavefunction collapse, *Proc. Natl. Acad. Sci. USA* **110**, 3777 (2013).
- [17] H. Katiyar, A. Brodutch, D. Lu, and R. Laflamme, Experimental violation of the Leggett-Garg inequality in a three-level system, *New J. Phys.* **19**, 023033 (2017).
- [18] K. Wang, C. Emary, X. Zhan, Z. Bian, J. Li, and P. Xue, Enhanced violations of Leggett-Garg inequalities in an experimental three-level system, *Opt. Express* **25**, 31462 (2017).
- [19] M. Tusun, W. Cheng, Z. Chai, Y. Wu, Y. Wang, X. Rong, and J. Du, Experimental violation of the Leggett-Garg inequality with a single-spin system, *Phys. Rev. A* **105**, 042613 (2022).
- [20] C. Emary, N. Lambert, and F. Nori, Leggett-Garg inequalities, *Rep. Prog. Phys.* **77**, 016001 (2014).
- [21] A. Kumari, M. D. Qutubuddin, and A. K. Pan, Violation of the Lüders bound of macrorealist and noncontextual inequalities, *Phys. Rev. A* **98**, 042135 (2018).
- [22] M. A. Nielsen and I. L. Chuang, *Quantum Computation and Quantum Information*, 10th anniversary ed. (Cambridge University Press, Cambridge, 2010).
- [23] J. D. Sivers and Q. Quraishi, Ion trap architectures and new directions, *Quant. Info. Proc.* **16**, 314 (2017).
- [24] J. Eschner, G. Morigi, F. Schmidt-Kaler, and R. Blatt, Laser cooling of trapped ions, *J. Opt. Soc. Am. B* **20**, 1003 (2003).
- [25] C. F. Roos, D. Leibfried, A. Mundt, F. Schmidt-Kaler, J. Eschner, and R. Blatt, Experimental Demonstration of Ground

- State Laser Cooling with Electromagnetically Induced Transparency, *Phys. Rev. Lett.* **85**, 5547 (2000).
- [26] G. Morigi, J. Eschner, and C. H. Keitel, Ground State Laser Cooling Using Electromagnetically Induced Transparency, *Phys. Rev. Lett.* **85**, 4458 (2000).
- [27] M. Zhang, Y. Xie, J. Zhang, W. Wang, C. Wu, T. Chen, W. Wu, and P. Chen, Estimation of the Laser Frequency Noise Spectrum by Continuous Dynamical Decoupling, *Phys. Rev. Appl.* **15**, 014033 (2021).
- [28] F. Schmidt-Kaler, S. Gulde, M. Riebe, T. Deuschle, A. Kreuter, G. Lancaster, C. Becher, J. Eschner, H. Häffner, and R. Blatt, The coherence of qubits based on single  $\text{Ca}^+$  ions, *J. Phys. B: At. Mol. Opt. Phys.* **36**, 623 (2003).
- [29] W. Nagourney, J. Sandberg, and H. Dehmelt, Shelved Optical Electron Amplifier: Observation of Quantum Jumps, *Phys. Rev. Lett.* **56**, 2797 (1986).
- [30] T. Sauter, W. Neuhauser, R. Blatt, and P. E. Toschek, Observation of Quantum Jumps, *Phys. Rev. Lett.* **57**, 1696 (1986).
- [31] J. C. Bergquist, R. G. Hulet, W. M. Itano, and D. J. Wineland, Observation of Quantum Jumps in a Single Atom, *Phys. Rev. Lett.* **57**, 1699 (1986).